ORIGINAL ARTICLE

Journal of Cachexia, Sarcopenia and Muscle 2022; **13**: 677–695
Published online 22 November 2021 in Wiley Online Library (wileyonlinelibrary.com) **DOI:** 10.1002/jcsm.12858

MyD88 deficiency ameliorates weight loss caused by intestinal oxidative injury in an autophagy-dependent mechanism

Ming Qi[1,2,3], Simeng Liao[1,3], Jing Wang[2], Yuankun Deng[2], Andong Zha[1,3], Yirui Shao[1,3], Zhijuan Cui[1,2], Tongxing Song[4], Yulong Tang[1]*, Bie Tan[2]* & Yulong Yin[1,2,3]

[1]*Laboratory of Animal Nutritional Physiology and Metabolic Process, Key Laboratory of Agro-ecological Processes in Subtropical Region, National Engineering Laboratory for Pollution Control and Waste Utilization in Livestock and Poultry Production, Institute of Subtropical Agriculture, Chinese Academy of Sciences, Changsha, Hunan, China;* [2]*College of Animal Science and Technology, Hunan Agricultural University, Changsha, Hunan, China;* [3]*University of Chinese Academy of Sciences, Beijing, China;* [4]*College of Animal Science and Technology, Huazhong Agricultural University, Wuhan, China*

Abstract

Background Gut health plays a vital role in the overall health and disease control of human and animals. Intestinal oxidative stress is a critical player in the induction and progression of cachexia which is conventionally diagnosed and classified by weight loss. Therefore, reduction of intestinal oxidative injury is a common and highly effective strategy for the maintenance of human and animal health. Here we identify intestinal myeloid differentiation primary response gene 88 (MyD88) as a novel target for intestinal oxidative stress using canonical oxidative stress model induced by paraquat (PQ) *in vitro* and *in vivo*.

Methods Intestinal oxidative stress was induced by administration of PQ in intestinal epithelial cells (IECs) and mouse model. Cell proliferation, apoptosis, DNA damage, mitochondrial function, oxidative status, and autophagy process were measured in wild-type and MyD88-deficient IECs during PQ exposure. Autophagy inhibitor (3-methyladenine) and activator (rapamycin) were employed to assess the role of autophagy in MyD88-deficient IECs during PQ exposure. MyD88 specific inhibitor, ST2825, was used to verify function of MyD88 during PQ exposure in mouse model.

Results MyD88 protein levels and apoptotic rate of IECs are increased in response to PQ exposure ($P < 0.001$). Intestinal deletion of MyD88 blocks PQ-induced apoptosis (~42% reduction) and DNA damage (~86% reduction), and improves mitochondrial fission (~37% reduction) and function including mitochondrial membrane potential (~23% increment) and respiratory metabolism capacity (~26% increment) ($P < 0.01$). Notably, there is a marked decrease in reactive oxygen species in MyD88-deficient IECs during PQ exposure (~70% reduction), which are consistent with high activity of antioxidative enzymes (~83% increment) ($P < 0.001$). Intestinal ablation of MyD88 inhibits mTOR signalling, and further phosphorylates p53 proteins during PQ exposure, which eventually promotes intestinal autophagy (~74% increment) ($P < 0.01$). Activation of autophagy (rapamycin) promotes IECs growth as compared with 3-methyladenine-treatment during PQ exposure (~173% increment), while inhibition of autophagy (3-methyladenine) exacerbates oxidative stress in MyD88-deficient IECs ($P < 0.001$). In mouse model, inhibition of MyD88 using specific inhibitor ST2825 followed by PQ treatment effectively ameliorates weight loss (~4% increment), decreased food intake (~92% increment), gastrocnemius and soleus loss (~24% and ~20% increment, respectively), and intestinal oxidative stress in an autophagy dependent manner ($P < 0.01$).

Conclusions MyD88 modulates intestinal oxidative stress in an autophagy-dependent mechanism, which suggests that reducing MyD88 level may constitute a putative therapeutic target for intestinal oxidative injury-induced weight loss.

Keywords Intestinal epithelial cells; Cachexia; Weight loss; DNA damage repair; Mitochondrial fission; Autophagy

Received: 23 March 2021; Revised: 7 October 2021; Accepted: 19 October 2021
*Correspondence to: Yulong Tang, Laboratory of Animal Nutritional Physiology and Metabolic Process, Key Laboratory of Agro-ecological Processes in Subtropical Region, National Engineering Laboratory for Pollution Control and Waste Utilization in Livestock and Poultry Production, Institute of Subtropical Agriculture, Chinese Academy of Sciences, Changsha 410125. Hunan, China. Email: tangyulong@isa.ac.cn
Bie Tan, College of Animal Science and Technology, Hunan Agricultural University, Changsha 410000, Hunan, China. Email: bietan@hunau.edu.cn

Introduction

Cachexia is a multifactorial syndrome diagnosed by body weight loss, weakness, and muscle atrophy.[1] Systemic inflammation and oxidative stress are commonly observed in patients with cachexia, having been postulated to play a key role in the diagnosis of the clinical symptoms.[2,3] Our previous study showed that oxidative stress resulted in poor growth performance and muscle damage in pig model.[4] In addition to muscle, multiple organs are participating to the pathogenesis in cachexia, including the intestinal tract, which is a key organ in immune and metabolism regulation.[5] As part of the immune response, intestinal epithelial cells (IECs) have developed a variety of functions which reduce the risk of infection or intoxication by microorganisms and toxic compounds.[6] Gut barrier dysfunction is a syndrome marked by failure of the gut epithelial barrier, with an increased gut permeability, morphological changes, accumulation of lymphocyte, and increased reactive oxygen species (ROS), leading to systemic inflammation.[7] Intestinal oxidative stress is an important factor in the occurrence and development of deteriorated intestinal barrier, which contribute to anorexia, muscle wasting, and severe weight loss in human and animals during cachexia.[1,8,9]

Disruption of redox homeostasis causes excessive generation of ROS, which are derived from respiratory chain of the inner mitochondrial membrane, resulting in oxidative damage of proteins, lipids, and nucleic acids in IECs.[6] Our previous studies illustrated that excessive ROS production resulted in increased apoptosis rate and decreased activity of antioxidative enzymes in IECs, which reduced appetite and body weight.[10] High ROS flux causes DNA strand breaks and mitochondrial dysfunction, including the disorder of electron respiratory chain (ETC) and a decrease in mitochondrial membrane potential (MMP).[11] Therefore, the normal mitochondrial function, oxidative DNA repair, and enzymatic antioxidants maintain cellular redox homeostasis, which are crucial in determining the potential human intestinal oxidative injury.[9]

Myeloid differentiation factor (MyD88) plays a pivotal role in directing the oxidative and inflammatory response to various stimuli, which is critical in the development of cancer cachexia.[12] Our previous transcriptome analysis showed significantly up-regulated jejunal expression of MyD88 in growth retarded piglets partially caused by oxidative stress, as characterized by poor appetite, gut barrier dysfunction, and impaired muscle regeneration.[8,13] Oxidative stress activates MyD88-dependent inflammatory signalling pathway resulting in high production of pro-inflammatory cytokines, and increased macrophage infiltration.[14,15] Transcription pattern identified TLR signalling involving MyD88 expression as activated in the murine keratinocytes under Paraquat (PQ)-induced ROS stress.[16] Autophagy can be regarded as a secondary defence to oxidative stress, by its ability to remove damaged substrates which may accumulate during this process.[6] Intestinal autophagy deficiency increases oxidative stress-induced apoptosis in intestinal IPEC-J2 cells.[6] MyD88-dependent inflammasome activation and autophagy inhibition contribute to intestinal oxidative stress injury.[17] PQ is a widely used herbicides and can be used as a ROS generator to produce experimental models of environmental oxidative stress.[18–21] PQ has been shown to cause severe weight loss, inappetence, and skeletal muscle degeneration.[22,23] It is generally accepted that accumulation of ROS and oxidative stress are responsible for PQ toxicity, leading to interruption of mitochondrial respiration chain, proteasomal damage, and cell death.[24] Considering that intestinal oxidative injury exaggerates cachexia,[25,26] PQ exposure is of great importance in understanding oxidative stress in IECs. In this study, we knock out *MyD88* in IECs and demonstrate the hypothesis that MyD88 deficiency ameliorates weight loss caused by intestinal oxidative injury through promoting autophagy *in vitro* and *in vivo*, which may provide an effective target for the clinical treatment of intestinal oxidative injury-induced cachexia.

Materials and methods

Reagents and antibodies

High-glucose (25 mM) Dulbecco's modified Eagle's (DMEM-H), foetal bovine serum (FBS), antibiotics (penicillin and streptomycin), and Lipofectamine2000 were obtained from Thermo Fisher Scientific. Methyl viologen dichloride hydrate (paraquat, PQ), dichloro-dihydro-fluorescein diacetate (DCFH-DA), DAPI, acridine orange (AO), dansylcadaverine (MDC), and NAO dye were purchased from Sigma (MO, USA). Rapamycin (RAPA) and 3-methyladenine (3-MA) were purchased from Selleckchem. ST2825 was purchased from MedChemExpress. All molecular biological reagents were obtained from New England Biolabs. Primary antibodies against mTOR, phosphor(P)-mTOR, P-p53, Drp1, Tom20,

cleaved-caspase 3, and Bcl-2 were purchased from Cell Signalling Technology. Anti-Ki67, phosphorylated histone H2A.X (P-γH2A.X), CD3, and CD68, and Alexa Fluor® 488-conjugated or Alexa Fluor® 594-conjugated second antibody were purchased from Abcam. Anti-LC3B, SQSTM1/P62, and MyD88 were purchased from Sigma. Anti-Beclin 1, CDK2, GPX1, 8-OHdG, OPA1, and Fis1 were purchased from Bioss (Woburn, MA, USA). Anti-SOD1, p53, PARP1, NDUFB8, and UQCRFS1 were purchased from Proteintech. Secondary antibodies horseradish peroxidase-conjugated goat anti-rabbit or mouse IgG was purchased from ZSGB-Bio.

Cell culture and transfection

The IPEC-J2 cells were grown in DMEM-H containing 10% FBS, 50 μg/ml penicillin, and 50 μg/ml streptomycin at 37°C in a 5% CO_2 incubator. The cells were transfected using Lipofectamine2000 at 70%–80% confluency according to the manufacturer's recommended protocol.

Double nicking CRISPR-Cas9

Guide RNAs were designed using the online CRISPR design tool (http://crispr.mit.edu/) and then cloned into the BbsI-digested plasmids (pSpCas9n) containing the entire guide RNA scaffold. After transfection, the genomic DNA of IPEC-J2 cells were extracted using Genomic DNA Miniprep kit (Axygen, AZ, USA). The genomic region flanking the MyD88 target site was amplified using polymerase chain reaction (PCR). The products underwent a re-annealing process to facilitate heteroduplex formation. After re-annealing, the products were treated with T7 Endonuclease I (T7E I) following the manufacturer's recommended protocol.

Isolation of clonal cell lines that were confirmed by T7E I were performed by serial dilutions. Detection of genomic microdeletions was performed by PCR sequencing. Off-target activity was analysed by deep sequencing and the Blast search (http://blast.ncbi.nlm.nih.gov/Blast.cgi).

Animals and experimental design

All animals used in this study were humanely managed according to the Chinese Guidelines for Animal Welfare. The experimental protocol was approved by the Animal Care and Use Committee of the Chinese Academy of Sciences (Beijing, China). A total of 32 male C57BL/6 mice aged 8 weeks were maintained at least one week before experiments. Mice were randomly distributed into 4 groups (n = 8 in each group): mice injected with normal saline (Ctrl); mice intraperitoneally injected with 30 mg/kg PQ (PQ); control mice administered with 25 mg/kg ST2825, a MyD88 specific inhibitor (ST); mice administered with 25 mg/kg ST2825 1 h before 30 mg/kg PQ injection (STPQ). At 24 h after PQ injection, all mice were sacrificed. Body weight, food intake, intestinal length, and weight were measured. Serum, jejunum, and the gastrocnemius (Gas) and soleus (Sol) samples were collected.

Cell viability assay

Cell proliferation assay

Cell proliferation was determined using cell counting kit CCK-8 according to the manufacturer's instructions (Dojindo, Osaka, Japan). IPEC-J2 cells were treated with PQ media for 12, 24, 36, and 48 h, respectively. Absorbance at 450 nm of each well was measured using a microplate reader (FLx800; BioTek Instruments, Inc.).

Cell cycle assay

Treated cells were collected and fixed in 70% ethanol overnight at 4°C. The cocktail solution (10 μl of Triton-X, 8 ml of PBS, 2 ml of RNAse A 1 mg/ml, and 200 μl of propidium iodide 1 mg/ml) was added to the cell pellet and incubated for 30 min at 20°C for analysis in a Beckman MoFlo XDP flow cytometer (Beckman Coulter, CA, USA).

Annexin V/PI staining assay

Following treatment, the cells were collected, and apoptosis was detected by flow cytometry using an Annexin V-FITC Apoptosis Detection Kit (Beyotime Biotechnology, Shanghai, China), following the manufacturer's instructions.

TUNEL assay

The paraffin-embedded jejunal sections and cell samples were detected using an In situ Cell-Death Detection Kit (Roche, Basel, Switzerland) following the manufacturer's instruction. The images of intestinal apoptotic rate were captured using a fluorescence microscope (Olympus) and analysed using Image Pro Plus software, Version 6.0 (IPP v6.0) (Media Cybernetics, Rockville, MD, USA).

Caspase 3 activity assay

Caspase 3 activity in cell and jejunal samples was measured with Caspase 3 Activity Assay Kit (Beyotime), determined by a colorimetric assay. The protein concentrations were measured using the Bradford Protein Assay Kit (Beyotime). Caspase 3 activity was normalized to protein concentration in parallel experimental plates.

Measurement of DNA damage using the comet assay

The comet assay was performed following the manufacturer's protocol (Trevigen, Gaithersburg, MD, USA). Briefly, DNA strand breaks of treated cells were separated by

electrophoresis in alkaline solution (200 mM NaOH, 1 mM EDTA, pH > 13) in a horizontal gel electrophoresis slide tray (Comet-10, Thistle Scientific, Glasgow, UK). The comets on the slides were stained and visualized with 20-μg/ml propidium iodide (Sigma-Aldrich, St. Louis, MO, USA). The slides were examined and images were captured using a Cytation™ five cell imaging multi-mode reader. Data are presented as mean tail moment compared with the control (non-treated cells).

Determination of mitochondrial function

Assessment of mitochondrial mass

After exposure to PQ, the treated cells at different time intervals (0, 24, 48 h) were washed with PBS to remove media content and were loaded with 5 μM of NAO dye and further incubated for 30 min. The treated cells were analysed using a fluorescence microscope (Olympus).

Mitotracker Red CMXRos staining

After treatment, cells were stained with 100 nM Mitotracker Red CMXRos (Thermo Fisher Scientific) dye at 37°C for 30 min. The fluorescent intensity of cells stained with Mitotracker Red CMXRos was analysed using a fluorescence microscope (Olympus).

Mitochondrial membrane potential (ΔΨm)

Changes in ΔΨm were assayed with JC-1 (Beyotime). The ΔΨm was calculated as the fluorescence ratio of aggregates (excitation/emission = 525/590 nm; red) to monomers (excitation/emission = 490/530 nm; green) using fluorescence microplate reader (FLx800; BioTek Instruments, Inc.).

Analysis of mitochondrial bioenergetics

The XF24 Analyser and XF Cell Mito Stress Test Kit (Seahorse Biosciences) were used for the mitochondrial bioenergetic analyses. At the end of each study, each well was sequentially injected Oligomycin (0.5 μM final concentration), carbonyl cyanide 4-(trifluoromethoxy) phenylhydrazone (FCCP, 1 μM final concentration), and rotenone/antimycin A (1 μM final concentration of each) and measured the oxygen consumption rate (OCR). Using these agents, we determined mitochondrial bioenergetics. Assays were analysed using the Seahorse XF Report Generator software (Wave, Agilent).

Evaluation of mitochondrial ETC activity

In our study, mitochondria were isolated from cell and jejunal samples with Mitochondria Isolation Kit (Beyotime). Then, the activity of Complex I and III in mitochondrial ETC was measured using Complex I Enzyme Activity Assay Kit (Abcam) and Mitochondrial Complex III Activity Assay Kit (Biovision, CA, USA) according to the manufacturer's instructions respectively.

ROS measurement and in situ superoxide detection

The ROS levels in cells and jejunal samples were evaluated by staining with DCFH-DA. Initially, cells and jejunal homogenate were stained with DCFH-DA, after which ROS-positive cells were measured using a Leica DMI4000B microscope (LEICA, Wetzlar, Germany) and a fluorescence microplate reader (Bio-Rad Laboratories). Dihydroethidium (DHE, 5 μM; Life Technologies) was used to detect superoxide in fresh frozen jejunal sections. Images were acquired under a fluorescence microscope (excitation/emission of 546/590 nm). The fluorescence intensity of jejunal sections was measured with ImageJ software (National Institutes of Health).

Indices of oxidative stress determination

Total superoxide dismutase (SOD) activities in collected cells and jejunal sections were determined using the Total Superoxide Dismutase Assay Kit (Beyotime) based on the protocols provided by the manufacturer. The contents of malondialdehyde (MDA), and activities of catalase (CAT) and glutathione per-oxidase (GSH-Px) were assessed using the corresponding commercial kits (Nanjing Jiancheng Bioengineering Institute, Nanjing, China) according to the instructions of the manufacturer. The protein concentration was determined using the BCA protein assay kit (Beyotime).

Determination of NAD^+/NADH levels

The colorimetric assay for NAD^+/NADH ratio determination was purchased from Biovision according to the manufacturer's protocols. Samples were spun and the supernatant was transferred to a 96-well plate for NAD+/NADH assays. Optical densities of the standard curve and samples were used to calculate NAD^+ content.

Assessment of ATP levels

Briefly, after treatments, cells and jejunal samples were harvested by trypsinization and collected in ice-cold PBS. Samples were determined for assessment of ATP levels using Enhanced ATP Assay Kit (Beyotime) according to the manufacturer's instructions. Data are represented as relative light units per milligram of protein.

Detection of autophagic vesicles

For detection of autophagic vesicles, cells were incubated with 1 μg/ml AO, or 50 μM MDC for 20 min at 37°C in a 5% CO_2 incubator. Then, they were washed three times in the ice-cold PBS. Fluorescence was recorded at 488/525 nm

(excitation/emission) for AO, and 380/525 nm (excitation/emission) for MDC using flow cytometry (Beckman, USA). Fluorescence was imaged using a fluorescence microscope (Olympus).

Transmission electron microscopy analysis

Treated cells and jejunal samples were fixed, washed, and post-fixed. After which cells were dehydrated and embedded in EPOK 812 (Oukenn, Tokyo, Japan). Then samples were post-stained with uranyl acetate and lead citrate at room temperature for 20 min. The stained cell and jejunal samples were then analysed using a TEM (H-600IV; Hitachi High-Technologies Corp.; Japan). Images were analysed using IPP v6.0 (Media Cybernetics).

Enzyme-linked immunosorbent assay

The concentrations of serum hormones including glucagon-like peptide-1 (GLP-1), peptide YY (PYY) and insulin-like growth factor 1 (IGF-1), D-lactate and cytochrome C (cyt c), and activities of diamine oxidase (DAO), lactase, sucrase, and maltase were determined by commercial pig or mouse enzyme-linked immunosorbent assay (ELISA) kits (Jiangsu Meimian industrial Co., Ltd, Jiangsu, China) according to the manufacturer's protocols. The concentrations of serum IL-1β, IL-6, TNF-α, and IFN-γ were analysed using mouse commercial ELISA kits (Cusabio Life Science Inc., Wuhan, China). The activity of myeloperoxidase (MPO) was determined following manufacturer's instruction (Nanjing Jiancheng Linc., Jiangsu, China). 8-OHdG levels were quantified with the OxiSelect Oxidative DNA Damage ELISA kit (Cell Biolabs, San Diego, CA, USA) according to manufacturer's instructions.

Intestinal morphology

The jejunal morphology were analysed using haematoxylin–eosin (H&E) staining. The images were captured and measured with computer-assisted microscopy (Micrometrics TM; Nikon ECLIPSE E200, Tokyo, Japan).

Segments of jejunum at higher magnification were analysed using scanning electron microscopy. Treated samples were examined by a JEOL JSM-6360LV scanning electron microscope at 25 KV. The apparent characteristics of microvillus were observed and described in the results.

Alcian blue and periodic acid-Schiff staining

The fixed segments were embedded in paraffin, and thin sections were obtained and stained with an alcian blue and periodic acid-Schiff (AB-PAS) stain kit (Abcam) according to the manufacturer's instruction. The stained sections were reviewed independently by two investigators using a microscope (Olympus, Tokyo, Japan), and scored by IPP v6.0 (Media Cybernetics).

Immunofluorescence

The cell samples and jejunal segments were blocked, and then incubated with primary antibodies overnight at 4°C. Then the slices were incubated with Alexa Fluor® 488-conjugated or Alexa Fluor® 594-conjugated second antibody (1:400) for 1 h at 37 °C. The nuclei were stained with DAPI. The images were captured and measured using fluorescence microscope (Olympus) and IPP v6.0 (Media Cybernetics).

Real-time quantitative PCR

RNA extraction and real-time quantitative PCR (RT-qPCR) were conducted according to previously study.[8] Primer pairs were listed in *Supporting information*, *Table S3*. The relative expression levels of the selected genes that were normalized by *β-actin* were calculated by using the $2^{-\triangle\triangle Ct}$ method.

Western blot analysis

The treated cells and jejunal tissues were lysed in ice cold lysis buffer with a complete protease inhibitor cocktail, and immunoblotting assays were performed. Protein band density was normalized to the β-actin signal and quantified using Quantity One software (Bio-Rad, Hercules, CA, USA).

Statistical analysis

Unpaired Student's *t* test and one-way analysis of variance (ANOVA) with Bonferroni correction were performed using SPSS software 20.0 (SPSS Inc., Chicago, IL, USA). Unless otherwise specified, all data were expressed as means ± standard error of mean (SEM). *P* values <0.05 were considered statistically significant. Data were expressed as the relative values to control group.

Results

PQ leads to apoptosis of IECs

As shown in *Figure* 1A, viability assay of IPEC-J2 cells was performed by treating the cells with different concentrations of PQ (35, 70 and 140 μM, respectively) for 12, 24, 36, and

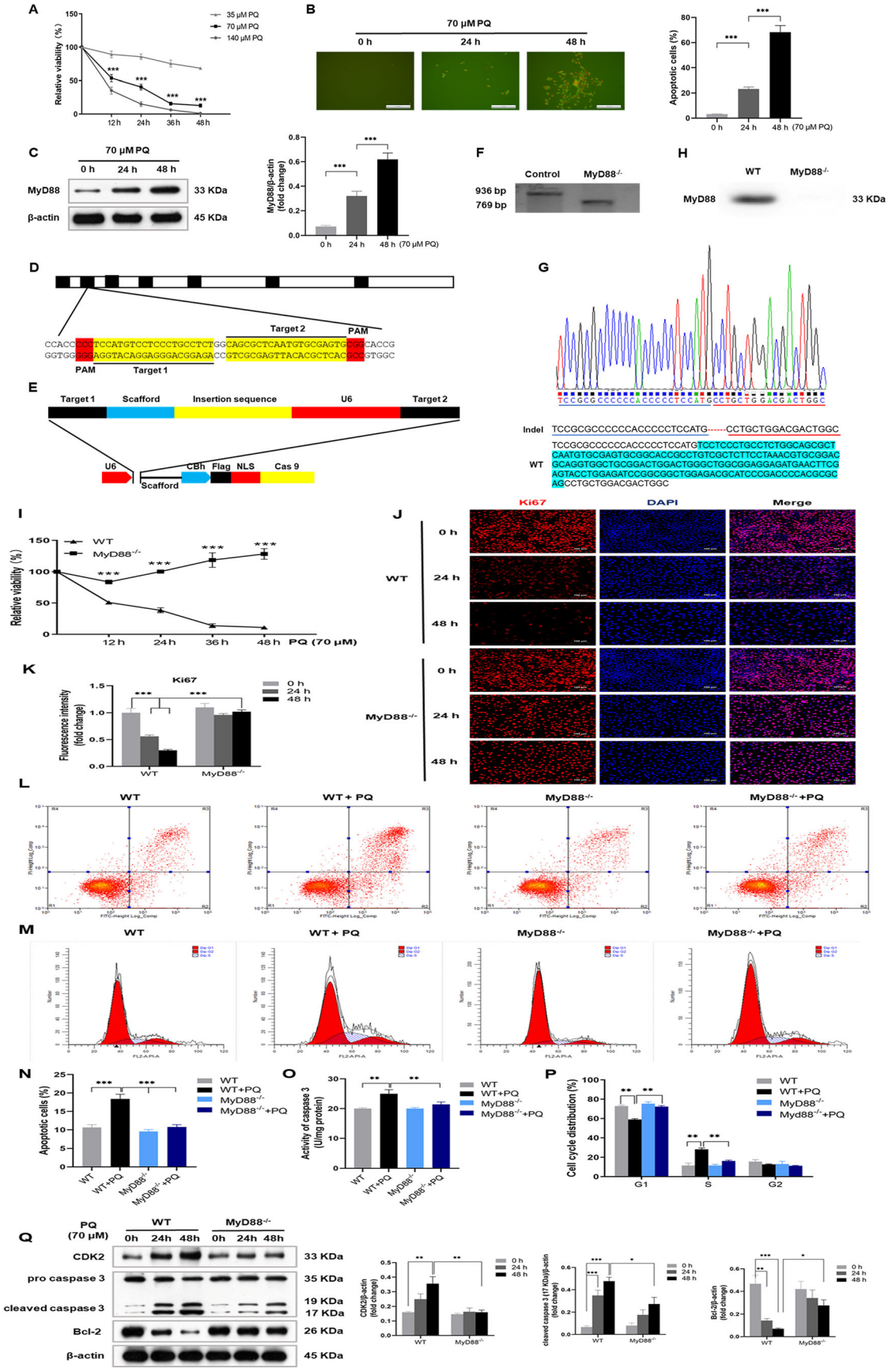
A
Relative viability (%)
35 μM PQ
70 μM PQ
140 μM PQ
12 h
24 h
36 h
48 h
B
70 μM PQ
0 h
24 h
48 h
Apoptotic cells (%)
0 h
24 h
48 h (70 μM PQ)
C
70 μM PQ
0 h
24 h
48 h
MyD88
β-actin
33 KDa
45 KDa
MyD88/β-actin (fold change)
F
Control
MyD88-/-
936 bp
769 bp
H
WT
MyD88-/-
MyD88
33 KDa
D
Target 2
PAM
PAM
Target 1
E
Target 1
Scafford
Insertion sequence
U6
Target 2
U6
CBh
Flag
NLS
Cas 9
Scafford
G
Indel
TCCGCGCCCCCCACCCCCTCCATG----CCTGCTGGACGACTGGC
WT
I
WT
MyD88-/-
Relative viability (%)
12 h
24 h
36 h
48 h
PQ (70 μM)
J
Ki67
DAPI
Merge
WT
MyD88-/-
0 h
24 h
48 h
K
Ki67
Fluorescence intensity (fold change)
0 h
24 h
48 h
WT
MyD88-/-
L
WT
WT + PQ
MyD88-/-
MyD88-/- +PQ
M
WT
WT + PQ
MyD88-/-
MyD88-/- +PQ
N
Apoptotic cells (%)
WT
WT+PQ
MyD88-/-
MyD88-/- +PQ
O
Activity of caspase 3 (U/mg protein)
WT
WT+PQ
MyD88-/-
MyD88-/- +PQ
P
Cell cycle distribution (%)
G1
S
G2
WT
WT+PQ
MyD88-/-
Myd88-/- +PQ
Q
PQ (70 μM)
WT
MyD88-/-
0h
24h
48h
CDK2
pro caspase 3
cleaved caspase 3
Bcl-2
β-actin
33 KDa
35 KDa
19 KDa
17 KDa
26 KDa
45 KDa
CDK2/β-actin (fold change)
cleaved caspase 3 (17 KDa)/β-actin (fold change)
Bcl-2/β-actin (fold change)

Figure 1 MyD88 deficiency ensures intestinal epithelial cells survival against PQ in vitro. (A) CCK8 assay was conducted to assess the viability of IPEC-J2 cells after 12, 24, 36, and 48 h of different concentrations of PQ treatment. (B) Fluorescence analysis of annexin V-FITC staining in the IPEC-J2 cells treated with PQ. (C) Protein expression of MyD88 in IPEC-J2 cells treated with PQ. (D) The *MyD88* gene was knocked out by two kinds of 20 bp 5′ targets (highlighted in yellow) followed by NGG (highlighted in black line). (E) A combinational sequence of two sets of targets, Scaffold and U6 were inserted into the plasmid (pSpCas9n(BB)) to knock out the *MyD88* gene. (F) Indels was induced by a pair of sgRNAs targeting the *MyD88* gene in the IPEC-J2 cells were assay by T7E I digestion. (G) The indels at *MyD88* gene were indicated in a sequence chromatogram. (H) Immunoblotting of MyD88 protein in WT and MyD88$^{-/-}$. (I) WT and MyD88$^{-/-}$ viability upon PQ exposure at 0, 12, 24, 36, and 48 h. (J,K) Representative images and quantification of Ki67 expression in WT and MyD88$^{-/-}$ against PQ. (L–N) Apoptotic rate and caspase 3 activity of WT and MyD88$^{-/-}$ against PQ for 24 h. (O,P) Cell cycle of WT and MyD88$^{-/-}$ against PQ for 24 h. (Q) Immunoblot and quantification of the CDK2, cleaved-caspase 3, and Bcl-2 in WT and MyD88$^{-/-}$ upon PQ exposure. Bacteria, plasmids and primers used for the PCR reaction are listed in *Table*s S1 and S2. Data represents the mean ± SEM. n = 3. *$P < 0.05$; **$P < 0.01$; ***$P < 0.001$ vs. control. WT, non-treated intestinal epithelial cells; MyD88$^{-/-}$, MyD88-deficient intestinal epithelial cells; PQ, paraquat.

48 h. Our results showed that the IPEC-J2 cells treated with PQ displayed reduced viability with time and dose increasing. The AnnexinV-FITC positive cell numbers were increased in PQ-treated cells (*Figure* 1B). PQ-treated IECs had a significantly increased protein abundance of MyD88 as compared with untreated cells (*Figure* 1C).

Knockout of the MyD88 gene by double-nicking CRISPR-Cas9 technology

To determine whether the blocked MyD88 expression contributes to attenuating PQ-induced intestinal epithelial injury, we attempted to knockout the *MyD88* gene in IECs (*Figure* 1D and –1G).

In order to avoid off-target double-stranded DNA breaks and indel formation in CRISPR-Cas9, we used the nickase version of Cas9 (Cas9n) with a pair of offset sgRNAs complementary to opposite strands of the target site (*Figure* 1D) and combined the two sgRNAs into a plasmid with scaffold, insertion sequence, and U6 (*Figures* 1E and S1A). The T7 Endonuclease I assay demonstrated that the cells transfected with the plasmid containing the two different sgRNAs harboured induced insertions and deletions (indels) (*Figure* 1F). Sanger sequencing of several single clonal cells, confirmed by T7 Endonuclease I, showed MyD88 to have been disrupted, as also confirmed by RT-qPCR results at transcript level (*Figures* 1G and S1B). Immunoblot assay further confirmed that a single clone that did not react with the anti-MyD88 antibodies was selected and maintained in the medium (*Figure* 1H) as the MyD88$^{-/-}$. Normal IPEC-J2 cell line was named as WT. We next examined the off-target activity in the MyD88$^{-/-}$ cells. The four possible off-target sites were selected for analysis, and the sequence assays showed that there were no off-targets in these sites (data not shown).

Intestinal deletion of MyD88 ensures IECs survival against PQ

WT and MyD88$^{-/-}$ cells showed the same proliferation rate (data not shown). As shown in *Figure* 1I–1K, PQ showed significantly less cytotoxicity to MyD88$^{-/-}$ cells than to WT with time increasing, which was also confirmed by the increased Ki67-positive cells and decreased cell apoptotic death in MyD88$^{-/-}$ cells (*Figure* 1I–1L,1N). The decreased mRNA and protein levels of cleaved-caspase 3 and Bcl-2, and activity of caspase 3 were observed in MyD88$^{-/-}$ (*Figures* 1O and 1Q and S2Aand S2B). MyD88$^{-/-}$ ameliorated PQ-induced cell cycle arrest, along with the up-regulated protein abundance of CDK2 (*Figure* 1M,1P, and 1Q).

Ablation of MyD88 alleviates PQ-induced DNA damage and mitochondrial dysfunction

Comet assay showed PQ exposure induced a significant increment in mean tail moment in WT, which was ameliorated in MyD88$^{-/-}$ cells (*Figure* 2A). PQ exposure significantly increased 8-OHdG accumulation, which was accordance with higher protein abundance of P-γH2A.X and lower protein abundance of PARP1 at 24 and 48 h in WT (*Figure* 2B and 2C). MMP was significantly decreased, as well as increased swollen mitochondria number but reduced total mitochondria number per area during PQ treatment in WT as compared in MyD88$^{-/-}$ cells. (*Figure* 3A–3C). PQ exposure significantly increased mRNA and protein abundance of Drp1, but downregulated protein expression of Tom20 and mRNA expression of *OPA1*, which was confirmed by NAO dye results (*Figures* 3D and 3E and S2C–S2E). PQ exposure dramatically decreased basal respiration, ATP production, maximal respiration, spare capacity, proton leak, and non-mitochondrial respiration, which was effectively reversed by MyD88 deficiency (*Figure* 3F).

Knockout of MyD88 decreases cellular ROS levels against PQ

Compared with WT, the accumulation of ROS and MDA was significantly reduced, while the activity of SOD, CAT, and GSH-Px was significantly increased in the MyD88$^{-/-}$ cells during PQ exposure. This result was accordance with the higher mRNA expression and protein abundances of SOD1

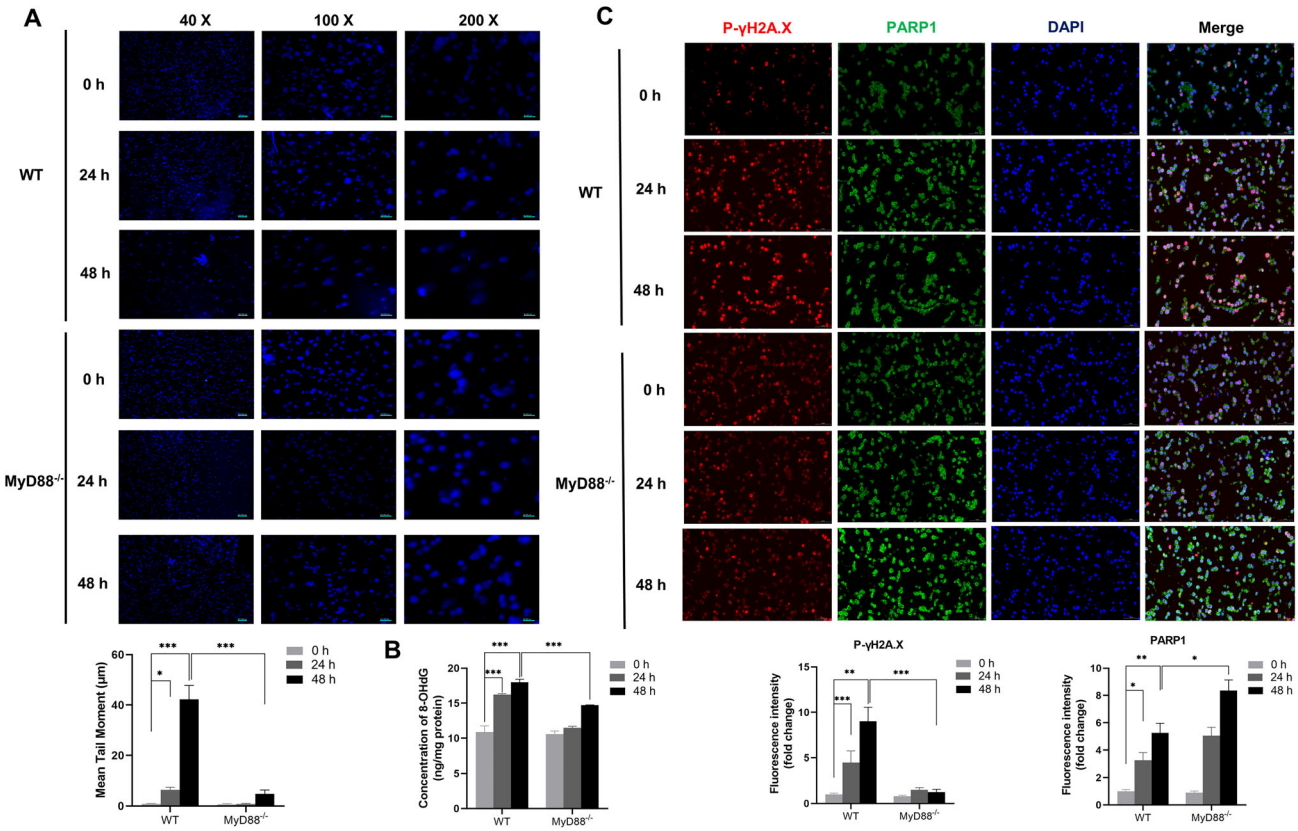

Figure 2 Intestinal deletion of MyD88 alleviates PQ-induced DNA damage. (A) Comet assay was used to detect DNA strand break in in WT and MyD88$^{-/-}$ against PQ. (B) Cellular concentration of 8-OHdG in WT and MyD88$^{-/-}$ against PQ. (C) Representative images and quantification of P-γH2A.X and PARP1 in WT and MyD88$^{-/-}$ against PQ. Data represent the mean ± SEM. n = 3. *$P < 0.05$; **$P < 0.01$; ***$P < 0.001$ vs. control. WT, non-treated intestinal epithelial cells; MyD88$^{-/-}$, MyD88-deficient intestinal epithelial cells; PQ, paraquat.

and GPX1 in MyD88$^{-/-}$ cells (*Figures* 4A–4C and S2F and S2G). The activities of mitochondrial ETC complex I and III were also reversed in MyD88$^{-/-}$ cells during PQ exposure (*Figure* 4D).

Intestinal ablation of MyD88 ensures cell survival against PQ through promotion of autophagy

The autophagy process was determined using TEM, AO, and MDC staining. We found higher number of autophagic vesicles in MyD88$^{-/-}$ cells compared with WT whether PQ treated or not (*Figure* 4E, 4F, and 4I). In accordance with this result, the increased mRNA expression and protein abundances of LC3B, Beclin 1, P-p53, and decreased protein abundances of P62, and P-mTOR were observed in MyD88$^{-/-}$ cells as compared with WT during PQ exposure (*Figures* 4J and S2H–S2J). Intestinal inhibition of MyD88 significantly increased ratio of NAD^+ to NADH and ATP levels as compared with WT during PQ exposure (*Figure* 4G and 4H).

Inhibition of autophagy exaggerates PQ-induced oxidative damage in MyD88-deficient cells

A 5 mM 3-MA (autophagy inhibitor) and a 5 μM RAPA (autophagy activator) were employed in MyD88$^{-/-}$ cells. Our results showed that 3-MA-treatment significantly reduced cell viability, associated with reduced Ki67-positive and higher TUNEL-positive cells during PQ exposure for 24 h (*Figure* 5A–5C). TEM analysis showed less and more autophagic vesicles in 3-MA-treated and RAPA-treated MyD88$^{-/-}$ cells, respectively. The mRNA expression and protein abundances of LC3B, P62, Beclin 1, and P-p53 showed same trend in accordance with TEM results (*Figures* 5D and 5Eand S3A–S3C). PQ treatment increased concentration of 8-OHdG in 3-MA-treatment, which accompanied by up-regulated protein level of P-γH2A.X and down-regulated PARP1 as compared with those in other two groups (*Figure* 6A–6C). In addition, PQ exposure increased swollen mitochondria number and reduced MMP in 3-MA-treatment, which was accompanied by increased protein and mRNA levels Drp1 and Fis1, and decreased OPA1 and Tom20 (*Figure* 6D–6G) in

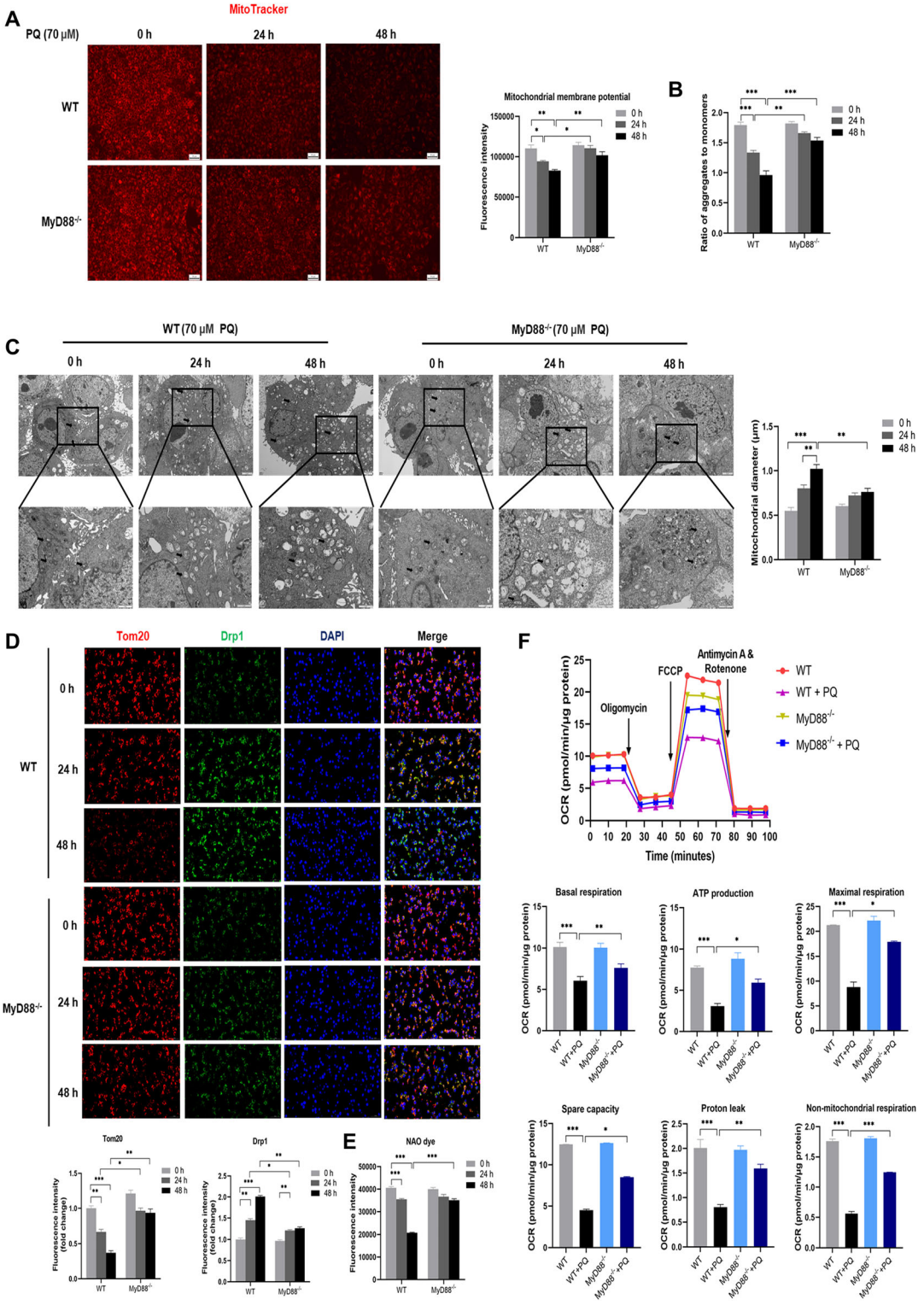

Figure 3 Ablation of MyD88 alleviates PQ-induced mitochondrial dysfunction. (A) MitoTracker was used to detect mitochondrial membrane potential in WT and MyD88$^{-/-}$ against PQ. (B) The ratio of aggregates to monomers in WT and MyD88$^{-/-}$ against PQ. (C) Representative transmission electron microscopy images and quantification of mitochondrial diameter in WT and MyD88$^{-/-}$ against PQ (marked with black arrows). (D) Representative images and quantification of Tom20 and Drp1 in WT and MyD88$^{-/-}$ against PQ. (E) NAO dye was used to detect mitochondrial number in WT and MyD88$^{-/-}$ against PQ. (F) Oxygen consumption rate was used to determine mitochondrial bioenergetics in WT and MyD88$^{-/-}$ against PQ. Data represent the mean ± SEM. $n = 3$. *$P < 0.05$; **$P < 0.01$; ***$P < 0.001$ vs. control. WT, non-treated intestinal epithelial cells; MyD88$^{-/-}$, MyD88-deficient intestinal epithelial cells; PQ, paraquat.

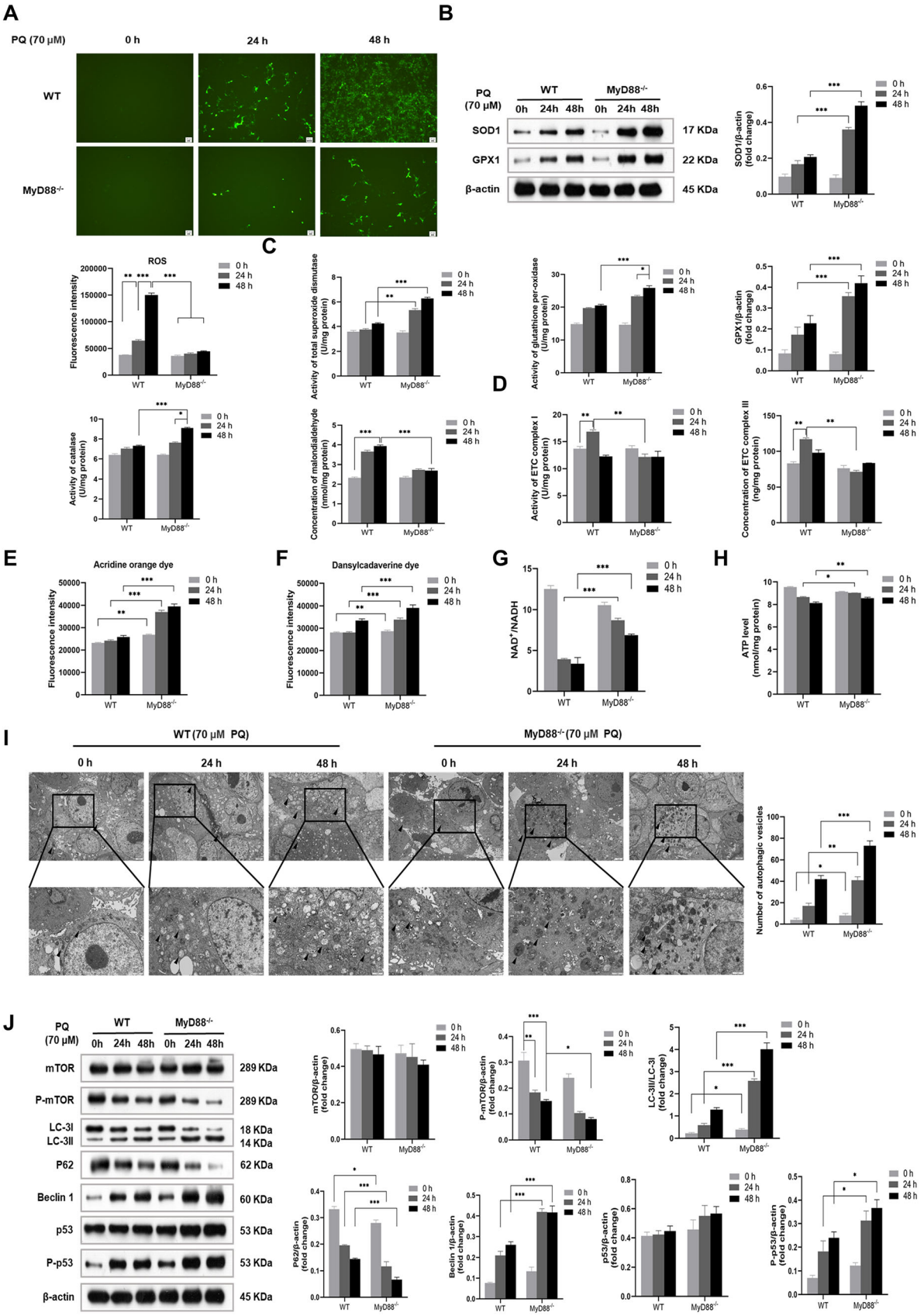

DOI: 10.1002/jcsm.12858

Figure 4 Knockout of MyD88 decreases PQ-induced ROS through promotion of autophagy. (A) Representative images and quantification of DCFH-DA-stained cells. (B) Western blot analysis of SOD1 and GPX1 in WT and MyD88$^{-/-}$ against PQ. (C) Antioxidative system in WT and MyD88$^{-/-}$ against PQ. (D) Determination of activity of ETC complex I and III in WT and MyD88$^{-/-}$ against PQ. (E) Quantification of acridine orange-stained cells. (F) Quantification of dansylcadaverine-stained cells. (G) Determination of NAD^+/NADH in WT and MyD88$^{-/-}$ against PQ. (H) Cellular ATP level in WT and MyD88$^{-/-}$ against PQ. (I) Representative transmission electron microscopy images and quantification of autophagic vesicles in WT and MyD88$^{-/-}$ against PQ (marked with black triangle). (J) Protein expression involved in autophagy process in WT and MyD88$^{-/-}$ against PQ. Data represents the mean ± SEM. $n = 3$. $^*P < 0.05$; $^{**}P < 0.01$; $^{***}P < 0.001$ vs. control. WT, non-treated intestinal epithelial cells; MyD88$^{-/-}$, MyD88-deficient intestinal epithelial cells; PQ, paraquat.

3-MA-treatment as compared with those in MyD88$^{-/-}$ and RAPA-treatment during PQ exposure (*Figures* 6H and 6I and S3D–S3F).

Inhibition of autophagy increases cellular ROS levels against PQ in MyD88-deficient cells

Inhibition of autophagy in MyD88$^{-/-}$ significantly increased cellular ROS levels, accompanied by overactivated ETC complex I and III during PQ exposure (*Figure* 6J and 6L). The decreased activities of antioxidative enzymes and increased concentration of MDA were observed in 3-MA-treatment compared with those in both RAPA-treatment and MyD88$^{-/-}$ cells during PQ exposure (*Figure* 6K), which was consistent with the results of relative mRNA expression of *SOD1* and *GPX1* (*Figure* 3G and 3H).

Inhibition of MyD88 alleviates PQ-induced intestinal damage in mouse model

The mouse experimental design was shown in *Figure* 7A. Intestinal inhibition of MyD88 by ST2825 significantly attenuated PQ-induced weight loss, decreased food intake, and Gas and Sol loss in mice. ST2825 treatment also increased gastrointestinal tract and intestinal content weight during PQ exposure (*Figures* 7A and 7B, S4A–S4G, and S7A). The mRNA expression of *MuRF1*, *MAFbx*, *FOXO1*, and *Atrogin 1* in Gas and Sol was decreased in STPQ group as compared with PQ group (*Figure* S4N and S4O). Inhibition of MyD88 significantly decreased serum levels of GLP-1 and PYY, and increased IGF-1 level (*Figure* S4H–S4J). PQ significantly decreased the ratio of villus height to crypt depth and goblet cells number and deteriorated structure of jejunal villi in jejunum, which was lined with decreased jejunal concentration of D-lactate and activity of DAO (*Figure* 7C–7E). IECs proliferation capacity was decreased during PQ exposure, which was accordance with the increased jejunal activity of caspase 3 and cyt c. PQ exposure also decreased jejunal digestive enzyme activities. However, STPQ effectively alleviated PQ-induced damaged jejunal barrier function (*Figures* 7F and 7G and S4K–S4M).

The STPQ significantly decreased mRNA expression and protein abundances of Drp1 and Fis 1 compared with PQ group. Increased MMP, mRNA, and protein abundance of OPA1 and lower number of swollen mitochondria were observed in STPQ compared with those in PQ group (*Figures* 7H–7K and S7B–S7D). Besides, PQ significantly increased concentration of 8-OHdG and protein levels of P-γH2A.X and decreased PARP1 expression at both mRNA and protein levels compared with Ctrl and ST (*Figures* 7L–7M and S7E).

The increased serum concentration of pro-inflammatory cytokines (IL-1β, IL-6, TNF-α, and IFN-γ) and jejunal activity of MPO, and higher jejunal mRNA expression of these pro-inflammatory cytokines were observed in PQ group. The jejunal $CD3^+$-positive and $CD68^+$-positive cells were significantly increased, which was confirmed by mRNA expression of *CD68* and *MCP1* in PQ group. The jejunal inflammation was ameliorated in STPQ group (*Figures* S5 and S6). PQ treatment significantly increased jejunal ROS and MDA levels, and activities of ETC complex I and III, and reduced activities of antioxidative enzymes compared with those in Ctrl and ST. However, STPQ significantly ameliorated jejunal oxidative stress compared with PQ group (*Figure* 8A–8D).

Increased jejunal ATP levels and number of autophagic vesicles were observed in STPQ group compared with that in PQ group. The jejunal mRNA expression and protein abundances of LC3B, Beclin 1, and P-p53 were significantly increased, and P62 was decreased in STPQ group compared with that in PQ group (*Figures* 8E–8H and S7F–S7H).

Discussion

There is a negative correlation between the degree of cachexia and patient survival; however, the aetiology of cachexia is not fully understood yet. It is today clear that oxidative stress and its-induced excessive inflammation play central roles in the syndrome, and the small intestine is the major tissue in nutrient absorption and immune response compared with other tissues in the body.[5] It is currently known that cachexia induces intestinal barrier dysfunction. The gut-derived components (such as LPS) trigger inflammatory response through activating the TLRs/MyD88-dependent pathway, which leads to weight loss and muscle wasting.[5,8,26] We found that oxidative stress increased apoptotic rate and protein abundance of MyD88 in IECs and intestinal MyD88 deficiency ameliorated weight loss caused by ROS-induced intestinal oxidative injury involving mitochondrial dysfunction

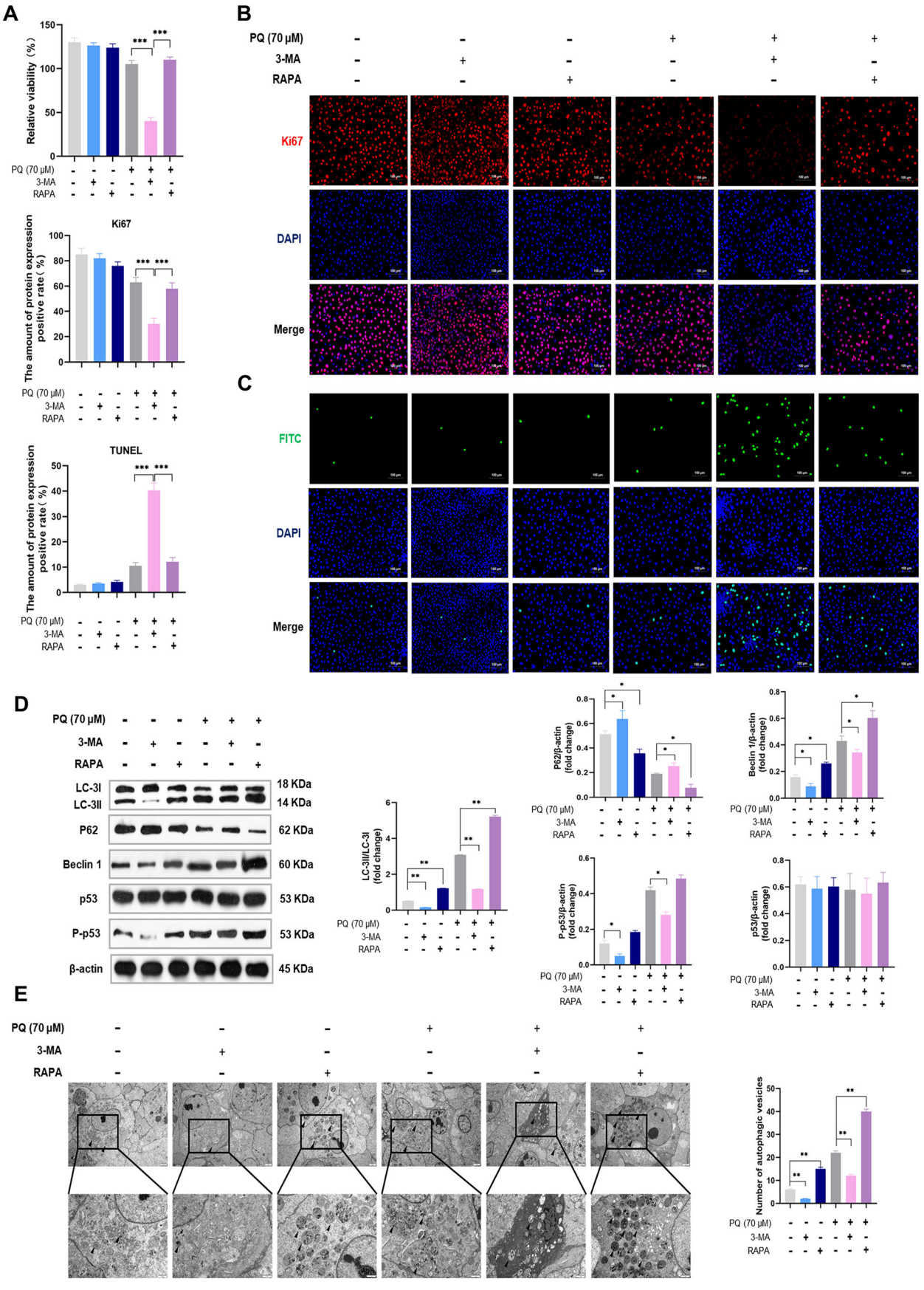

DOI: 10.1002/jcsm.12858

Figure 5 Inhibition of autophagy aggravates PQ-induced cell death in MyD88-deficient cells. (A) Cell viability in 3-MA-treated and RAPA-treated MyD88$^{-/-}$ against PQ. (B) Representative images and quantification of Ki67 expression in 3-MA-treated and RAPA-treated MyD88$^{-/-}$ against PQ. (C) TUNEL analysis of apoptotic rate of 3-MA-treated and RAPA-treated MyD88$^{-/-}$ against PQ. (D) Protein expression involved in autophagy process in 3-MA-treated and RAPA-treated MyD88$^{-/-}$ against PQ. (E) Representative transmission electron microscopy images and quantification of autophagic vesicles in 3-MA-treated and RAPA-treated MyD88$^{-/-}$ against PQ (marked with black triangle). Data represent the mean ± SEM. $n = 3$. *$P < 0.05$; **$P < 0.01$; ***$P < 0.001$ vs. control. MyD88$^{-/-}$, MyD88-deficient intestinal epithelial cells; PQ, paraquat; 3-MA, 3-methyladenine; RAPA, rapamycin.

and DNA damage through promoting intestinal autophagy *in vitro* and *in vivo* (*Figure* 9).

Loss of body weight (including muscle mass) and inappetence are common morbidities that often appear earlier than other symptoms in cachexia.[12] In mouse model, we showed that inhibition of MyD88 improved oxidative stress-induced weight loss, Gas and Sol muscle loss, and decreased food intake. It may be explained by downregulated gene expression of muscle protein degradation and recovered serum appetite-related hormones level, which is similar to that found in a murine sarcoma model,[27] suggesting that these features of cachexia are sensitive to MyD88 signalling blockade. Intestinal disturbance is one of the major factors contributing to the loss of weight mass and muscle wasting.[1,28] A recent study performed in cachectic rats showed the significantly reduced weight of the caecal and stomach content, and accelerated gastric emptying.[1] This study corroborates our finding that the weight of intestine and average faeces was decreased during PQ exposure while intestinal blockage of MyD88 rescued the loss. The augmented proliferation of IECs responds to intestinal oxidative injury, which was observed in the intestinal crypts of cachectic patients compared with the weight stable cancer patients.[29] In the present study, the MyD88$^{-/-}$ cells improved cell proliferation and rescued cell cycle arrest as compared with WT during PQ exposure. It is suggested that intestinal *MyD88* deficiency acts as cellular defence pathway against the damaging effects of PQ, which is accordance with the results in our mouse model. The impaired jejunal integrity induces poor ability of nutrient absorption, which is observed in patients with cachexia.[30] We found that inhibition of MyD88 improved activity of jejunal digestive enzymes in mice suffered from intestinal oxidative injury. Intestinal integrity is also required in intestinal immune function. MyD88 inhibitor ameliorated the defects in the mucus barrier in PQ-treated mice, which is accordance with depletion of goblet cells in the colon epithelium in cachectic patients, compared with weight stable counterparts.[5] The impaired mucus barrier triggers systemic inflammation and cytokine storms in the course of the cachexia process, which already occur in patients.[5] We found that intestinal inhibition of MyD88 decreased production of pro-inflammatory cytokines in PQ-treated mice, which agrees with the increased colonic concentration of cytokines in the cancer cachectic patients.[5] The increased level of pro-inflammatory cytokines is associated with activated macrophages and T cells, which is responsible for causing cachexia syndrome.[7] We found PQ induced recruitment of immune cells including CD68$^+$ and CD3$^+$-positive immune cells in mice model, which was rescued by inhibition of MyD88. This study evidenced an increase in the macrophage population and persistence of CD3$^+$ T cells in cachectic patients.[31] It is suggested that intestinal inhibition of MyD88 ameliorates PQ-induced weight loss caused by intestinal barrier dysfunction and excessive inflammation in mice model.

Oxidative stress deteriorates intestinal barrier and induces systemic inflammation in cachectic patients with skeletal muscle loss.[25,26] Accumulation of DNA damage-induced mutations is considered a significant mediator of progression of cachexia.[11] Oxidative DNA damage was observed in the hearts of cachectic mice.[32] We found decreased protein expression of DNA damage marker (P-γH2A.X) and concentrations of 8-OHdG, and increased protein expression of PARP1 in MyD88$^{-/-}$ cells during PQ exposure. It is suggested that intestinal MyD88 deficiency promotes DNA damage repair under PQ exposure, which contributes to ameliorating cachexia-associated syndrome. Similar results have also been observed in previous study that DNA damage induced by ultraviolet radiation was less pronounced in MyD88-deficient mice compared with wild-type mice, which reduced weight loss in mice.[33] The oxidative stress-induced mitochondrial dysfunction causes skeletal muscle atrophy in progression of cachexia in mice with weight loss.[34] Our results showed that intestinal knockout of MyD88 effectively alleviated PQ-induced mitochondrial dysfunction involving decreased intestinal MMP, increased mitochondrial fission, and aggravated mitochondrial bioenergetics. These results agree with previous study that LPS induced abnormal mitochondrial fusion–fission and pro-inflammatory response in mice with severe weight loss, while inhibition of NF-κB pathway quenched oxidative injury.[17] Another study also found the lower mitochondrial biogenesis, associated with activated nuclear translocation of pro-inflammatory NF-κB in cachectic rat with skeletal muscle abnormalities.[35] Reducing ROS level by antioxidative enzyme system attenuates oxidative damage of cellular components, contributing to decreasing occurrence of cachexia.[11,25] The ROS-induced muscle contractile dysregulation was observed in SOD1$^{-/-}$ mice as compared with wild-type mice.[25] Our results showed intestinal MyD88 deficiency decreased level of ROS and MDA, associated with inhibited overactivation of ETC complexes I and III, which are considered as major sources of ROS during PQ exposure. We further showed that the decreased cellular oxidative

DOI: 10.1002/jcsm.12858

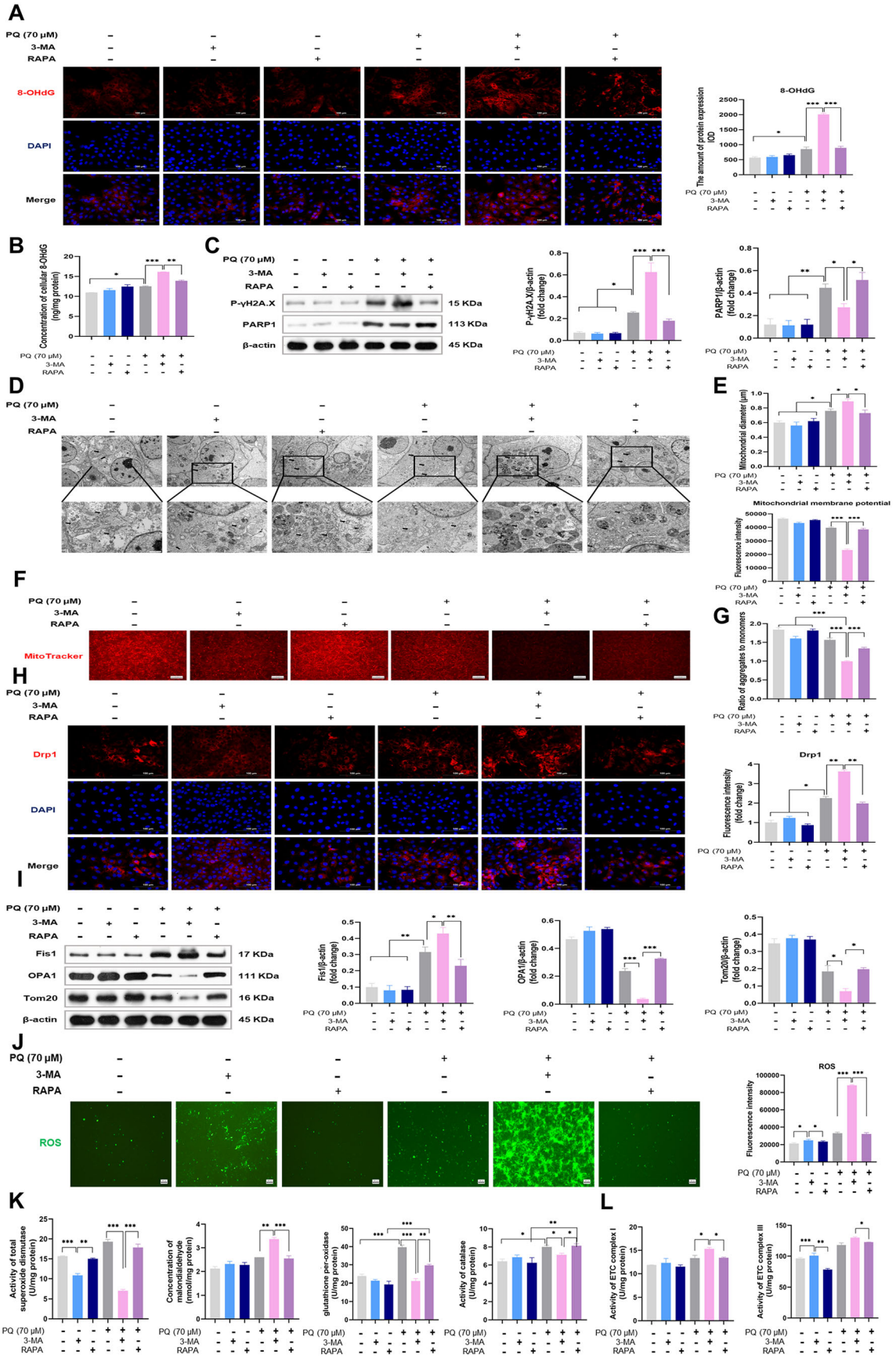

DOI: 10.1002/jcsm.12858

Figure 6 Inhibition of autophagy aggravates ROS-induced mitochondrial dysfunction and DNA damage in MyD88-deficient cells. (A) Representative images and quantification of 8-OHdG in 3-MA-treated and RAPA-treated MyD88$^{-/-}$ against PQ. (B) Concentration of cellular 8-OHdG in 3-MA-treated and RAPA-treated MyD88$^{-/-}$ against PQ. (C) Protein expression of P-γH2A.X and PARP1 in 3-MA-treated and RAPA-treated MyD88$^{-/-}$ against PQ. (D,E) Representative transmission electron microscopy images and quantification of mitochondrial diameter in 3-MA-treated and RAPA-treated MyD88$^{-/-}$ against PQ (marked with black arrows). (F) Mitochondrial membrane potential in 3-MA-treated and RAPA-treated MyD88$^{-/-}$ against PQ. (G) The ratio of aggregates to monomers in 3-MA-treated and RAPA-treated MyD88$^{-/-}$ against PQ. (H) Representative images and quantification of Drp1 expression in 3-MA-treated and RAPA-treated MyD88$^{-/-}$ against PQ. (I) Protein expression of Fis1, OPA1, and Tom20 in 3-MA-treated and RAPA-treated MyD88$^{-/-}$ against PQ. (J) Representative images and quantification of DCFH-DA-stained cells. (K) Antioxidative system in 3-MA-treated and RAPA-treated MyD88$^{-/-}$ against PQ. (L) Determination of activity of ETC complex I and III in 3-MA-treated and RAPA-treated MyD88$^{-/-}$ against PQ. Data represents the mean ± SEM. $n = 3$. *$P < 0.05$; **$P < 0.01$; ***$P < 0.001$ vs control. MyD88$^{-/-}$, MyD88-deficient intestinal epithelial cells; PQ, paraquat; 3-MA, 3-methyladenine; RAPA, rapamycin.

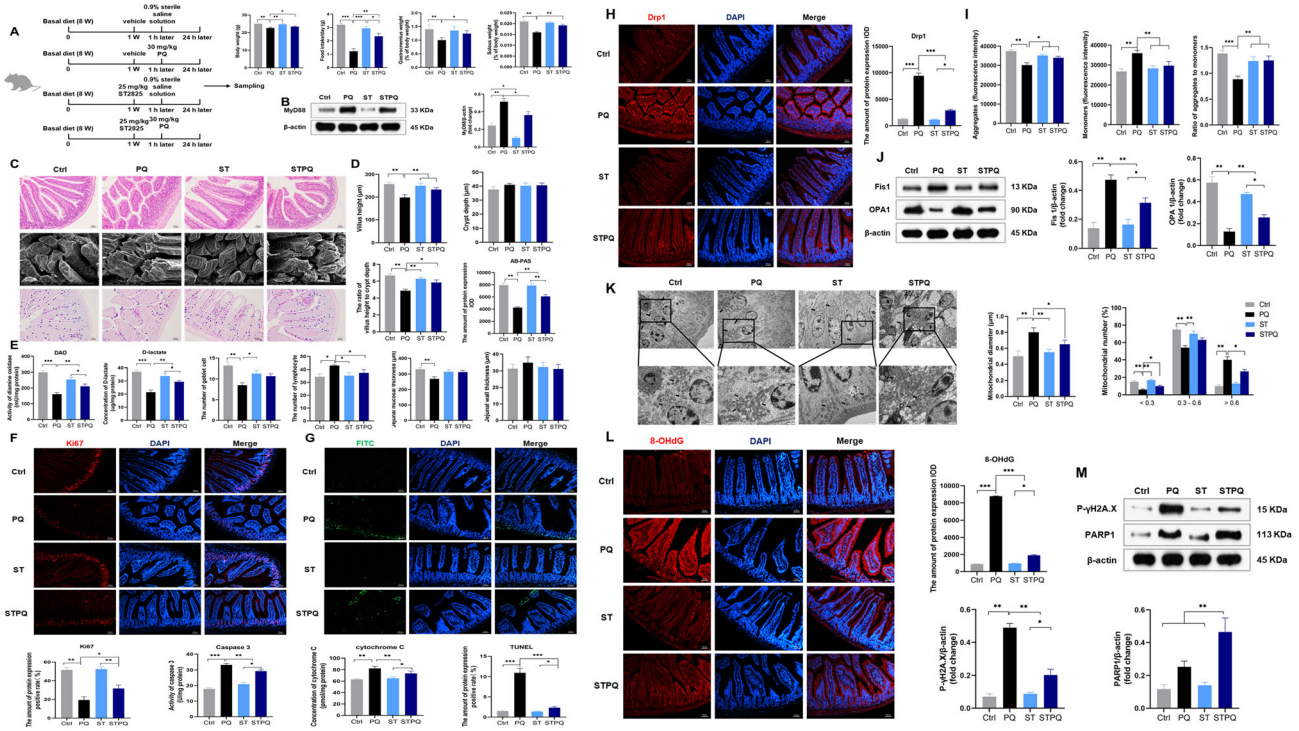

Figure 7 Inhibition of MyD88 expression alleviates PQ-induced intestinal damage *in vivo* through improving DNA damage and mitochondrial dysfunction. (A) The mouse experimental design, body weight, food intake, gastrocnemius, and soleus weight. (B) Protein expression of MyD88 in four groups. (C) Representative images of haematoxylin–eosin staining, scanning electron microscopy, alcian blue and periodic acid-Schiff staining of jejunum in four groups. (D) Quantification of jejunal morphology and alcian blue and periodic acid-Schiff-stained cells. (E) Quantification of jejunal permeability in four groups. (F) Representative images and quantification of jejunal Ki67 expression. (G) TUNEL analysis of jejunal apoptotic rate, activity of caspase 3, and cellular cytochrome c level in four groups. (H) Representative images and quantification of Drp1 expression in four groups. (I) The ratio of aggregates to monomers in four groups. (J) Protein expression of Fis1 and OPA1 in four groups. (K) Representative transmission electron microscopy images and quantification of mitochondrial diameter in four groups (marked with black arrows). (L) Representative images and quantification of 8-OHdG in four groups. (M) Protein expression of P-γH2A.X and PARP1 in four groups. Data represent the mean ± SEM. $n = 8$. *$P < 0.05$; **$P < 0.01$; ***$P < 0.001$ vs. control.

stress in MyD88$^{-/-}$ cells was dependent on antioxidative enzymes activation including SOD, CAT, and GSH-Px. These results are consistent with a recent study that SOD1-konck out aggravated pro-inflammatory response and oxidative damage in cachectic mouse with colitis, accompanied by disrupted activity of complexes I and III.[11,36] Down-regulated expression of MyD88 was also reported to promote antioxidative activity, and reversed LPS-stimulated ROS accumulation in macrophages of mice.[37] These *in vitro* findings were verified in the results *in vivo*. These findings suggest that intestinal inhibition of MyD88 ameliorates PQ-induced DNA damage and mitochondrial dysfunction, which is associated with enhanced activity of antioxidative enzymes and reduced production of ROS in IECs.

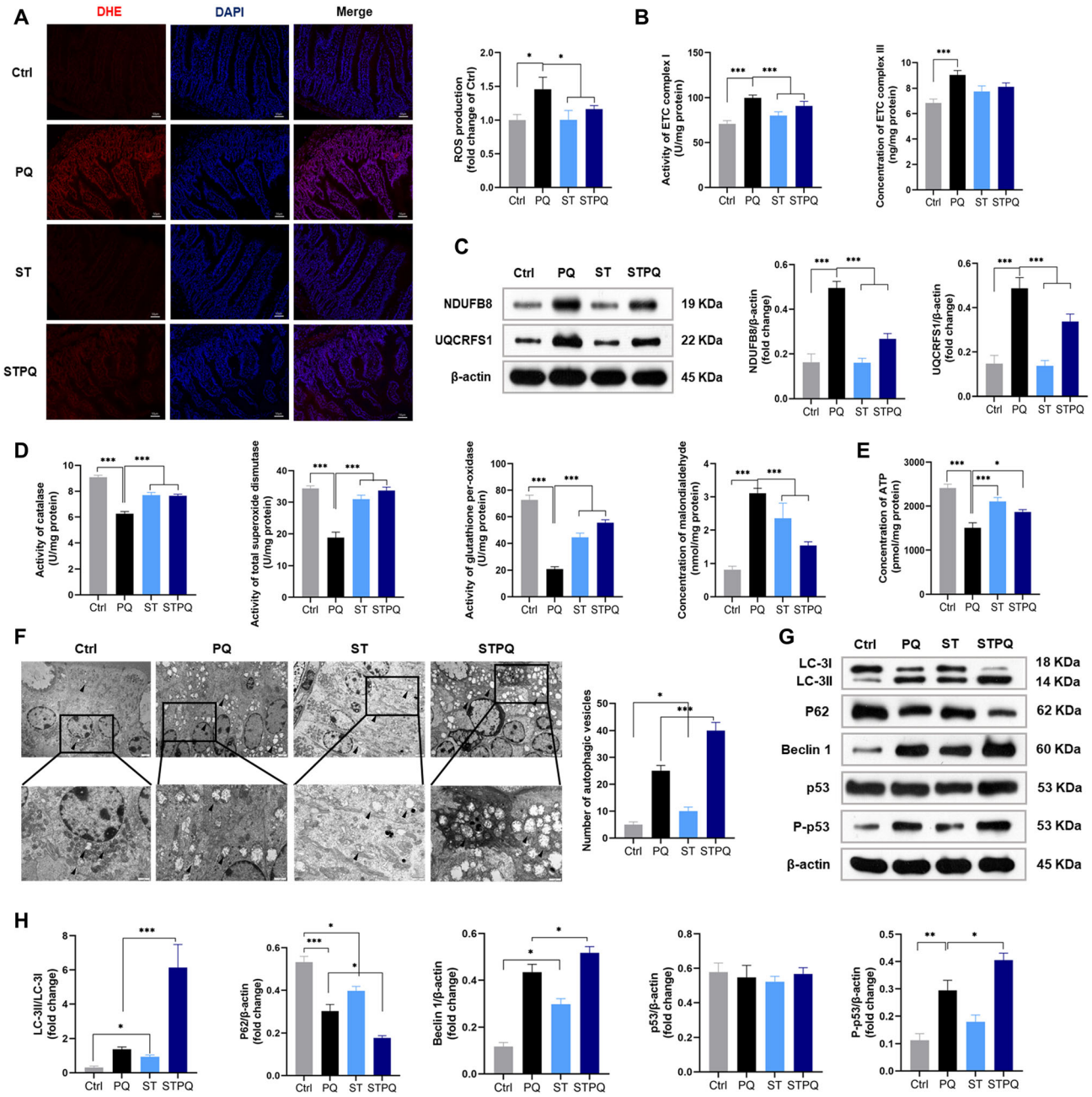

Figure 8 Inhibition of MyD88 expression decreases PQ-induced jejunal ROS through promotion of autophagy *in vivo*. (A) *In situ* superoxide detection in jejunum of four groups. (B) Determination of jejunal activity of ETC complex I and III in four groups. (C) Protein expression of ETC complex I and III in four groups. (D) Antioxidative system in four groups. (E) Cellular ATP level in four groups. (F) Representative transmission electron microscopy images and quantification of autophagic vesicles in four groups (marked with black triangle). (G,H) Protein expression involved in autophagy process in four groups. Data represent the mean ± SEM. n = 8. $^{*}P < 0.05$; $^{**}P < 0.01$; $^{***}P < 0.001$ vs. control.

Next, we determined the mechanism of intestinal MyD88 deficiency reducing ROS level in IECs during PQ exposure. The increased oxidative stress and cell death due to impaired autophagy were observed in cachectic patients with chronic heart failure.[38] Activation of autophagy is sufficient to prevent mitochondrial dysfunction and improve muscle regeneration in cachectic mice with muscle weakness.[39] In this study, a significant increase in autophagosome and protein abundances of autophagy-related protein were observed in MyD88$^{-/-}$ cells as compared with that in WT during PQ exposure, suggesting that intestinal knockout of MyD88 may defend against PQ toxicity through activating autophagy.

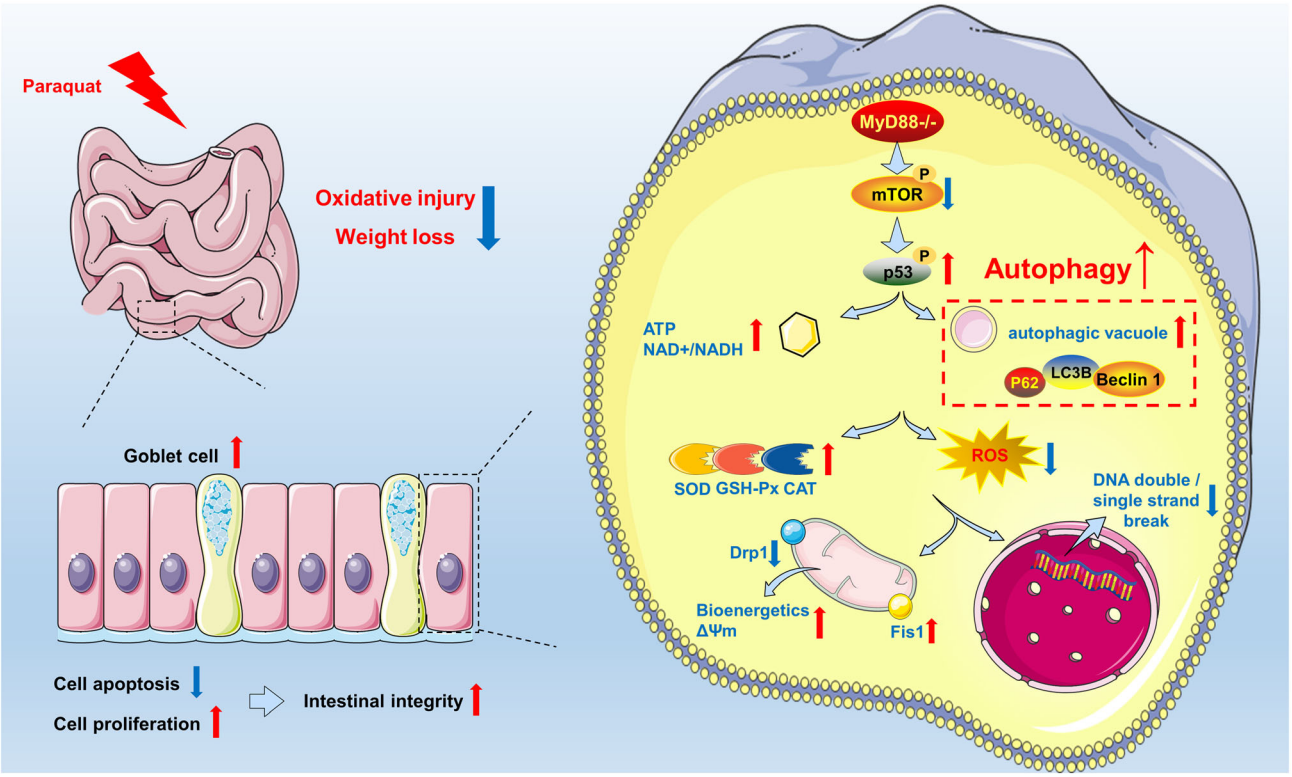

Figure 9 Proposed mechanisms underlying MyD88 deficiency ameliorates weight loss caused by ROS-mediated intestinal mitochondrial dysfunction and DNA damage through promoting autophagy.

It agrees with previous study that appropriate induction of autophagic process eliminated oxidative and endoplasmic reticulum stress, and maintained skeletal muscle mass during ageing and other cachexia syndromes.[3] In addition, PQ treatment significantly increased protein level of P-p53 and increased ratio of NAD^+ to NADH and ATP levels in $MyD88^{-/-}$ cells, which was in accordance with the previous study that ROS-induced DNA damage activated p53, and transcriptionally activated repair of DNA lesions in mice with low weight gain.[40] We further performed RAPA or 3-MA to activate or inhibit autophagy, respectively, in $MyD88^{-/-}$ cells. Our results showed that 3-MA-treatment caused severe cell death in $MyD88^{-/-}$ as compared with no-treatment and RAPA-treatment during PQ exposure. 3-MA-treatment aggravated PQ-induced cellular DNA damage and mitochondrial fission, which was associated with an increase in cellular ROS production and deteriorated activities of antioxidative enzymes. It is suggested that inhibition of autophagy in $MyD88^{-/-}$ cells exacerbated PQ-induced intestinal injury. However, the complex interplay between MyD88 signalling and autophagy needs to be further explored.

In conclusion, our findings demonstrate that intestinal MyD88 deficiency effectively ameliorated weight loss caused by ROS-induced DNA damage and mitochondrial dysfunction *in vitro* and *in vivo* in an autophagy-dependent pathway. MyD88 is expected to become a novel therapeutic target for the treatment of intestinal oxidative injury and provide effective reference and guidance for clinical prevention for intestinal oxidative stress-induced cachexia.

Acknowledgements

This work was supported by the National Natural Science Foundation of China (32072745 and 32130099) and Innovation Province Project (2019RS3021). The authors certify that they comply with the ethical guidelines for authorship and publishing of the *Journal of Cachexia, Sarcopenia and Muscle*.[41]

Online supplementary material

Additional supporting information may be found online in the Supporting Information section at the end of the article.

Figure S1. Double Nicking CRISPR-Cas9. A: The sequence contained a pair of sgRNA, scaffold, insertion sequence and U6 was cloned into plasmidpSpCas9n for knock out the MyD88 gene by double nicking method in the IPEC-J2 cells. **B:** Verification of MyD88 knockout on transcript level.

Figure S2. Relative mRNA expression of WT and MyD88$^{-/-}$ during PQ exposure. A-B: Relative mRNA expression of *caspase 3* and *Bcl-2*. **C-E:** Relative mRNA expression of *Drp1*, *Fis1*, and *OPA1*. **F-G:** Relative mRNA expression of *SOD1* and *GPX1*. **H-J:** Relative mRNA expression of *LC3B-II/LC3B-I*, *P62*, and *Beclin 1*. Data represents the mean ± SEM. n = 3. *$P < 0.05$; **$P < 0.01$; ***$P < 0.001$ vs control.

Figure S3. Relative mRNA expression of 3-MA-and RAPA-treated MyD88$^{-/-}$ during PQ exposure. A-C: Relative mRNA expression of *LC3B-II/LC3B-I*, *P62*, and *Beclin 1*. **D-F:** Relative mRNA expression of *Drp1*, *Fis1*, and *OPA1*. **G-H:** Relative mRNA expression of *SOD1* and *GPX1*. Data represents the mean ± SEM. n = 3. *$P < 0.05$; **$P < 0.01$; ***$P < 0.001$ vs control.

Figure S4. The physiological changes of intestine, muscle genes expression related to protein degradation, serum hormones, and jejunal digestive enzyme activity in mice challenged with PQ. A-G: The length and weight of gastrointestinal tract. **H-J:** Serum concentrations of appetite hormone GLP-1, IGF-1, and PYY. **K-M:** Intestinal activity of digestive enzymes. **N-O:** Relative mRNA expression involved in muscle protein degradation in gastrocnemius and soleus muscles. Data represents the mean ± SEM. n = 8. *$P < 0.05$; **$P < 0.01$; ***$P < 0.001$ vs control.

Figure S5. Serum and jejunal inflammatory markers in mice during PQ exposure. A-D: Serum concentrations of pro-inflammatory cytokines IL-1β, IL-6, TNF-α, and IFN-γ. **E-H:** The jejunal mRNA expression of *IL-1β*, *IL-6*, *TNF-α*, and *IFN-γ*. **I:** Jejunal MPO activity. Data represents the mean ± SEM. n = 8. *$P < 0.05$; **$P < 0.01$; ***$P < 0.001$ vs control.

Figure S6 Jejunal lymphocyte distribution in mice during PQ exposure. A-C: Representative images and quantification of $CD3^+$ and $CD68^+$-positive cells. **D-E:** Jejunal mRNA expression of *CD68* and *MCP1*. Data represents the mean ± SEM. n = 8. *$P < 0.05$; **$P < 0.01$; ***$P < 0.001$ vs control.

Figure S7 Relative mRNA expression of jejunum in mice during PQ exposure. A: mRNA expression of *MyD88*. **B-D:** mRNA expression of *Drp1*, *Fis1*, and *OPA1*. **E:** mRNA expression of *PARP1*. **F-H:** mRNA expression of *LC3B-II/LC3B-I*, *P62*, and *Beclin 1*. Data represents the mean ± SEM. n = 8. *$P < 0.05$; **$P < 0.01$; ***$P < 0.001$ vs control.

Table S1. Strain and plasmids for sgRNA clone.

Table S2. Primer sequence for sgRNA validation.

Table S3. Primer pairs used for quantitative reverse transcription-PCR.

Conflict of interest

The authors declare no conflict of interest.

References

1. Potgens SA, Thibaut MM, Joudiou N, Sboarina M, Neyrinck AM, Cani PD, et al. Multi-compartment metabolomics and metagenomics reveal major hepatic and intestinal disturbances in cancer cachectic mice. *J Cachexia Sarcopeni* 2021;**12**: 456–475.
2. Argiles JM, Busquets S, Lopez-Soriano FJ. Anti-inflammatory therapies in cancer cachexia. *Eur J Pharmacol* 2011;**668**: S81–S86.
3. Abrigo J, Elorza AA, Riedel CA, Vilos C, Simon F, Cabrera D, et al. Role of oxidative stress as key regulator of muscle wasting during cachexia. *Oxid Med Cell Longev* 2018;**2018**:1–17.
4. Wen C, Li F, Guo Q, Zhang L, Duan Y, Wang W, et al. Protective effects of taurine against muscle damage induced by diquat in 35 days weaned piglets. *J Anim Sci Biotechnol* 2020;**11**:56.
5. Costa RGF, Caro PL, de Matos-Neto EM, Lima J, Radloff K, Alves MJ, et al. Cancer cachexia induces morphological and inflammatory changes in the intestinal mucosa. *J Cachexia Sarcopenia Muscle* 2019;**10**: 1116–1127.
6. Tang Y, Li J, Li F, Hu CA, Liao P, Tan K, et al. Autophagy protects intestinal epithelial cells against deoxynivalenol toxicity by alleviating oxidative stress via IKK signaling pathway. *Free Radic Biol Med* 2015;**89**: 944–951.
7. Wyart E, Bindels LB, Mina E, Menga A, Stanga S, Porporato PE. Cachexia, a systemic disease beyond muscle atrophy. *Int J Mol Sci* 2020;**21**.
8. Qi M, Tan B, Wang J, Li J, Liao S, Yan J, et al. Small intestinal transcriptome analysis revealed changes of genes involved in nutrition metabolism and immune responses in growth retardation piglets1. *J Anim Sci* 2019;**97**:3795–3808.
9. Bhattacharyya A, Chattopadhyay R, Mitra S, Crowe SE. Oxidative stress: an essential factor in the pathogenesis of gastrointestinal mucosal diseases. *Physiol Rev* 2014;**94**: 329–354.
10. Zha A, Yuan D, Cui Z, Qi M, Liao S, Liao P, et al. The evaluation of the antioxidant and intestinal protective effects of baicalin-copper in deoxynivalenol-challenged piglets. *Oxid Med Cell Longev* 2020;**2020**:5363546.
11. Hoeijmakers JH. DNA damage, aging, and cancer. *N Engl J Med* 2009;**361**: 1475–1485.
12. Zhu XX, Burfeind KG, Michaelis KA, Braun TP, Olson B, Pelz KR, et al. MyD88 signalling is critical in the development of pancreatic cancer cachexia. *J Cachexia Sarcopeni* 2019;**10**:378–390.
13. Tao S, Zhou T, Saelao P, Wang Y, Zhu Y, Li T, et al. Intrauterine growth restriction alters the genome-wide DNA methylation profiles in small intestine, liver and longissimus dorsi muscle of newborn piglets. *Curr Protein Pept Sci* 2019;**20**: 713–726.
14. Reuter S, Gupta SC, Chaturvedi MM, Aggarwal BB. Oxidative stress, inflammation, and cancer: how are they linked? *Free Radic Biol Med* 2010;**49**:1603–1616.
15. Yang J, Liu H, Han S, Fu Z, Wang J, Chen Y, et al. Melatonin pretreatment alleviates renal ischemia-reperfusion injury by promoting autophagic flux via TLR4/MyD88/MEK/ERK/mTORC1 signaling. *FASEB J* 2020;**34**:12324–12337.
16. Song X, Narzt MS, Nagelreiter IM, Hohensinner P, Terlecki-Zaniewicz L, Tschachler E, et al. Autophagy deficient keratinocytes display increased DNA damage, senescence and aberrant lipid composition after oxidative stress in vitro and in vivo. *Redox Biol* 2017;**11**:219–230.
17. Zhou M, Xu W, Wang J, Yan J, Shi Y, Zhang C, et al. Boosting mTOR-dependent autophagy via upstream TLR4-MyD88-MAPK signalling and downstream NF-kappaB pathway quenches intestinal inflammation and oxidative stress injury. *EBioMedicine* 2018;**35**:345–360.

18. Reczek CR, Birsoy K, Kong H, Martinez-Reyes I, Wang T, Gao P, et al. A CRISPR screen identifies a pathway required for paraquat-induced cell death. *Nat Chem Biol* 2017;**13**: 1274−+.
19. Takizawa M, Komori K, Tampo Y, Yonaha M. Paraquat-induced oxidative stress and dysfunction of cellular redox systems including antioxidative defense enzymes glutathione peroxidase and thioredoxin reductase. *Toxicol In Vitro* 2007;**21**:355–363.
20. Aoki H, Otaka Y, Igarashi K, Takenaka A. Soy protein reduces paraquat-induced oxidative stress in rats. *J Nutr* 2002;**132**: 2258–2262.
21. Shibata M, Hakuno F, Yamanaka D, Okajima H, Fukushima T, Hasegawa T, et al. Paraquat-induced oxidative stress represses phosphatidylinositol 3-kinase activities leading to impaired glucose uptake in 3T3-L1 adipocytes. *J Biol Chem* 2010;**285**: 20915–20925.
22. Siegel MP, Wilbur T, Mathis M, Shankland EG, Trieu A, Harper ME, et al. Impaired adaptability of in vivo mitochondrial energetics to acute oxidative insult in aged skeletal muscle. *Mech Ageing Dev* 2012; **133**:620–628.
23. Takenaka A, Annaka H, Kimura Y, Aoki H, Igarashi K. Reduction of paraquat-induced oxidative stress in rats by dietary soy peptide. *Biosci Biotech Bioch* 2003;**67**: 278–283.
24. Gonzalez-Polo RA, Rodriguez-Martin A, Moran JM, Niso M, Soler G, Fuentes JM. Paraquat-induced apoptotic cell death in cerebellar granule cells. *Brain Res* 2004; **1011**:170–176.
25. Qaisar R, Bhaskaran S, Premkumar P, Ranjit R, Natarajan KS, Ahn B, et al. Oxidative stress-induced dysregulation of excitation-contraction coupling contributes to muscle weakness. *J Cachexia Sarcopenia Muscle* 2018;**9**:1003–1017.
26. Brown JL, Lawrence MM, Ahn B, Kneis P, Piekarz KM, Qaisar R, et al. Cancer cachexia in a mouse model of oxidative stress. *J Cachexia Sarcopenia Muscle* 2020;**11**: 1688–1704.
27. Ruud J, Backhed F, Engblom D, Blomqvist A. Deletion of the gene encoding MyD88 protects from anorexia in a mouse tumor model. *Brain Behav Immun* 2010;**24**: 554–557.
28. Van Krimpen SJ, Jansen FAC, Ottenheim VL, Belzer C, van der Ende M, van Norren K. The effects of pro-, pre-, and synbiotics on muscle wasting, a systematic review-gut permeability as potential treatment target. *Nutrients* 2021;**13**.
29. Ulmer TF, Rosch R, Mossdorf A, Alizai H, Binnebosel M, Neumann U. Colonic wall changes in patients with diverticular disease—Is there a predisposition for a complicated course? *Int J Surg* 2014;**12**: 426–431.
30. Konstam MA, Kiernan MS, Bernstein D, Bozkurt B, Jacob M, Kapur NK, et al. Evaluation and management of right-sided heart failure: a scientific statement from the american heart association. *Circulation* 2018;**137**:e578–e622.
31. Thiesen S, Janciauskiene S, Uronen-Hansson H, Agace W, Hogerkorp CM, Spee P, et al. CD14(hi)HLA-DR (dim) macrophages, with a resemblance to classical blood monocytes, dominate inflamed mucosa in Crohn's disease. *J Leukoc Biol* 2014;**95**:531–541.
32. Hinch EC, Sullivan-Gunn MJ, Vaughan VC, McGlynn MA, Lewandowski PA. Disruption of pro-oxidant and antioxidant systems with elevated expression of the ubiquitin proteosome system in the cachectic heart muscle of nude mice. *J Cachexia Sarcopenia Muscle* 2013;**4**:287–293.
33. Harberts E, Zhou H, Fishelevich R, Liu J, Gaspari AA. Ultraviolet radiation signaling through TLR4/MyD88 constrains DNA repair and plays a role in cutaneous immunosuppression. *J Immunol* 2015;**194**: 3127–3135.
34. Brown JL, Rosa-Caldwell ME, Lee DE, Blackwell TA, Brown LA, Perry RA, et al. Mitochondrial degeneration precedes the development of muscle atrophy in progression of cancer cachexia in tumour-bearing mice. *J Cachexia Sarcopenia Muscle* 2017; **8**:926–938.
35. Barazzoni R, Gortan Cappellari G, Palus S, Vinci P, Ruozi G, Zanetti M, et al. Acylated ghrelin treatment normalizes skeletal muscle mitochondrial oxidative capacity and AKT phosphorylation in rat chronic heart failure. *J Cachexia Sarcopenia Muscle* 2017;**8**:991–998.
36. Hwang J, Jin J, Jeon S, Moon SH, Park MY, Yum DY, et al. SOD1 suppresses pro-inflammatory immune responses by protecting against oxidative stress in colitis. *Redox Biol* 2020;**37**:101760.
37. He J, Han S, Li XX, Wang QQ, Cui Y, Chen Y, et al. Diethyl blechnic exhibits anti-inflammatory and antioxidative activity via the TLR4/MyD88 signaling pathway in LPS-stimulated RAW264.7 cells. *Molecules* 2019;**24**:4502.
38. Yin JY, Lu X, Qian ZY, Xu WT, Zhou X. New insights into the pathogenesis and treatment of sarcopenia in chronic heart failure. *Theranostics* 2019;**9**:4019–4029.
39. Baraldo M, Geremia A, Pirazzini M, Nogara L, Solagna F, Turk C, et al. Skeletal muscle mTORC1 regulates neuromuscular junction stability. *J Cachexia Sarcopenia Muscle* 2020;**11**:208–225.
40. De Zio D, Cianfanelli V, Cecconi F. New insights into the link between DNA damage and apoptosis. *Antioxid Redox Signal* 2013; **19**:559–571.
41. von Haehling S, Morley JE, Coats AJS, Anker SD. Ethical guidelines for publishing in the *Journal of Cachexia, Sarcopenia and Muscle*: update 2019. *J Cachexia Sarcopenia Muscle* 2019;**10**:1143–1145.